MATERIALS
CHARACTERIZATION

Microstructural and compositional study of a bulk $Pb(Mg_{1/3}Nb_{2/3})O_3-PbTiO_3$ single crystal grown from a $BaTiO_3$ seed

Zoran Samardžija [a,*], Jae-Ho Jeon [b], Miran Čeh [a]

[a] *Institite »Jožef Stefan«, Jamova 39, SI-1000 Ljubljana, Slovenia*
[b] *Korea Institute of Machinery and Materials, 66 Sangnam-Dong, Changwon, South Korea*

Abstract

The microstructure, composition and homogeneity of a $Pb(Mg_{1/3}Nb_{2/3})O_3-PbTiO_3$ (PMNT) single crystal were studied using a combination of electron-microprobe techniques: scanning electron microscopy, orientation analysis and quantitative X-ray microanalysis. A PMNT single crystal was grown from a polycrystalline PMNT matrix using a $BaTiO_3$ single crystal as a seed. The PMNT crystal retained the same crystallographic orientation as the seed with no interdiffusion at the interface. The average chemical composition, determined with optimized quantitative wavelength-dispersive X-ray microanalysis, was $Pb(Mg_{1/3}Nb_{2/3})_{1-x}Ti_xO_3$ where $x = 0.33$. A statistical evaluation of the data using the analysis of variance showed that the achieved experimental uncertainty was below $\pm 1\%$ relative. The compositional homogeneity of the crystal was verified on the micrometer-scale; however on the macro-scale slight fluctuations of the Mg, Nb and Ti concentrations were observed across the crystal. The measured variations from the average composition were $\pm 2.3\%$ relative for Ti, $\pm 1.3\%$ for Nb and $\pm 1.4\%$ for Mg. In contrast, the Pb concentration was found to be uniform on both the micro- and macro-scale, showing a variation below $\pm 0.5\%$ relative.
© 2006 Elsevier Inc. All rights reserved.

Keywords: Microanalysis; PMNT; Microstructure; Compositional homogeneity

1. Introduction

Single crystals from solid solutions from $Pb(Mg_{1/3}Nb_{2/3})O_3$ (PMN) and $PbTiO_3$ (PT), PMNT, have been extensively investigated as ferroelectric materials that exhibit superior electromechanical properties, such as high piezoelectric coefficients ($d_{33} > 2000$ pC/N), large strain levels ($>0.6\%$), high dielectric constants (from 1000 to 5000) and low dielectric losses ($<1\%$) [1,2].

Other advantages of PMNT, compared to similar relaxor-based solid solutions, are the high stability of its perovskite structure and its low affinity for the formation of the undesirable pyrochlore phase [3,4]. Such single crystals have a great potential for various advanced piezo-applications, for example, high-performance ultrasonic transducers and actuators. The enhanced piezoelectric properties of this material are related to the morphotropic phase-boundary (MPB) effects, where the formation of macro-domains occurs due to the partial substitution of Ti^{4+} for complex $(Mg_{1/3}Nb_{2/3})^{4+}$ on the B-site [3]. The MPB composition for the $(1-x)PMN-xPT$ system corresponds to $x \approx 0.35$, where

* Corresponding author. Tel.: +386 1 4773847.
  E-mail address: zoran.samardzija@ijs.si (Z. Samardžija).

the solid solution changes structure from the rhombohedral to the tetragonal [4]. In most cases the composition of PMNT materials is adjusted to be similar or close to the MPB region, where the piezoelectric properties achieve their maximum. Further engineering of the properties in MPB-based ceramics by means of a compositional adjustment of the Curie temperature has also been reported [1]. Slight compositional variations can, therefore, significantly influence the piezoelectricity and the domain-structure arrangement [4,5]. Because the properties are sensitive to a fluctuation in the composition, this issue has to be carefully considered during the crystal-preparation process in order to maintain the homogeneity of the crystal and/or to avoid segregation effects. Compositional studies have usually been performed on large PMNT single crystals on the meso-scale (mm) using X-ray fluorescence (XRF) or laser ablation inductively coupled plasma (ICP) mass spectrometry [6,7]. In some studies the electron-probe microanalysis (EPMA) was applied on the mm-scale, but with a considerable experimental uncertainty of $\geq \pm 3\%$ relative [4] or for a qualitative analysis only [2].

In this work an advanced EPMA study with the emphasis on high analytical sensitivity, high precision and accuracy was applied to determine the chemical composition and to evaluate the micro- and macro-homogeneity of the PMNT single-crystal sample. The PMNT single crystal was prepared from a polycrystalline PMNT matrix using the templated grain-growth (TGG) method with a $BaTiO_3$ (110) single crystal as the seed [2,8]. The microstructure and orientation of the grown PMNT crystal were investigated with scanning electron microscopy and electron backscatter diffraction (EBSD). Qualitative and quantitative elemental analyses were carried out using energy-dispersive X-ray spectroscopy (EDXS) and optimized wavelength-dispersive X-ray spectroscopy (WDXS). The compositional homogeneity was studied by measuring the variations of the cation concentrations on both the micro- and macro-scale using WDXS with an appropriate experimental sampling design. The data were statistically evaluated with the analysis of variance approach (ANOVA).

2. Experimental

Weighed powders of $MgNb_2O_6$, PbO and TiO_2 were mixed by ball-milling and then calcined at 800 °C for 6 h in air to form the $Pb(Mg_{1/3}Nb_{2/3})_{0.70}Ti_{0.30}O_3$ (PMNT) powder precursor. The synthesized PMNT powder was mixed with an excess of 8 mol% of PbO and pressed into green compacts in a die of 16-mm

diameter using uniaxial pressing and subsequent cold isostatic pressing at 200 MPa. The excess of PbO was added in order to compensate for PbO loss during sintering, to promote single crystal growth and to prevent the formation of undesirable pyrochlore phases [2,4]. The green compacts were pre-sintered at 1000 °C for 10 min using the double enclosed crucible method, and $PbZrO_3$ powder was used to fill the spaces between the crucibles to reduce the weight loss due to the evaporation of PbO. In order to produce PMNT single crystals, a $BaTiO_3$ single-crystal seed (Ceracomp Co., Ltd., South Korea) was placed on the pre-sintered PMNT polycrystalline sample and then heat-treated again at 1150 °C for 50 h in a double enclosed alumina crucible.

For the EPMA a cross-section of the PMNT–$BaTiO_3$ specimen was prepared by a conventional metallographic technique, which included grinding and polishing with different graded diamond pastes. The final polishing was performed with 0.25-μm paste. The same polishing procedure was applied to standard reference materials. Both, the sample and the standards were evaporated together with ~ 20-nm-thick carbon coating to avoid charging under the electron beam.

Preliminary examination of the microstructure, qualitative and semi-quantitative analyses were carried out in a JEOL JSM 5800 scanning electron microscope (SEM) equipped with an Oxford-Link ISIS 300 EDXS system with an ultra-thin window Si(Li) detector. The operating conditions for the SEM/EDXS were 20-kV accelerating voltage, ~ 0.5-nA beam current and 35° take-off angle. The EBSD patterns for the orientation analysis were recorded in a Philips-FEI XL30 environmental scanning electron microscope (ESEM) with an HKL Channel 5 EBSD technology system. To enhance the pattern quality, the sample surface was gently re-polished and the conductive carbon layer removed. In this case the surface charging was eliminated by using controlled water pressure (50 to 100 Pa) in the ESEM. The patterns were acquired at a 20-kV accelerating voltage and ~ 5-nA beam current.

The quantitative microanalysis was carried out in a JEOL JXA 840A electron-probe microanalyzer equipped with two wavelength-dispersive (WD) spectrometers controlled by a Tracor Series II X-ray Analysis System. The issue of standard reference materials for the quantitative analysis was carefully considered. In order to minimize matrix effects and to improve analytical accuracy we tried to avoid the use of pure metallic standards or glass compounds. For that reason appropriate, stable stoichiometric oxide compounds were preferred as standards for the analysis of

the complex PMNT oxide ceramics. Pure sintered polycrystalline PbO and Nb_2O_5 pellets and single crystals of MgO and $SrTiO_3$ were used as standards for the quantification of the Pb, Nb, Mg and Ti, respectively, whereas the oxygen content was calculated from the stoichiometry according to the nominal cation valencies.

Because of the relatively low mass fraction of Mg in the PMNT a large absorption of the "soft" Mg-$K\alpha$ radiation ($E=1.254$ keV) in the heavy PMNT matrix is expected. This can introduce an additional error, arising from the calculations within quantitative matrix-correction programs [9]. In order to decrease the absorption effect the microanalysis should be carried out at lower primary electron-beam energies. The Monte Carlo calculations, performed with CASINO program [10,11], were used to estimate the size of electron interaction volume and the $\Phi(\rho z)$ X-ray depth–distribution curves for various beam energies. The results demonstrate a significant reduction of the absorption as well as an improved spatial resolution at lower beam energies, as shown in Fig. 1. For the analysis of the complex PMNT sample an acceleration voltage of 15 kV was chosen for our measurements as a good compromise. This gives a sufficient overvoltage ratio and ionization yield for all cations and an acceptable degree of absorption for the Mg.

The X-ray intensities for the Pb-$M\alpha$, Nb-$L\alpha$ and Ti-$K\alpha$ spectral lines were measured on a PET crystal with a Xe-filled sealed proportional counter, whereas the Mg-$K\alpha$ line was measured on a TAP crystal and a gas-flow (P-10 gas) proportional counter. The WDXS measurements were performed using focused point-beam analysis at a beam current of 60 nA and take-off angle of 40°. Several measurements at 10 kV and 100 nA were undertaken to test the influence of the absorption

correction on the quantitative results. For all the analyses the beam current was monitored with Faraday cup readings prior to the start of each new point data acquisition. With a properly aligned and saturated tungsten filament, the beam current was very stable, with a measured drift of less than 1% relative over a period of 5 h. Even so, for a consistent statistical evaluation, all X-ray raw-counts data were corrected for current drift.

Accurate peak (P) and background (B) positions were determined from precise, slow wavelength scans on standards and additionally re-checked on the PMNT sample. It was found that two peaks from multiple-λ reflections ($n=2$) of Pb-$M\alpha$ and Pb-$M\beta$ radiation were located in the vicinity of the Mg-$K\alpha$ peak. For this reason, the background positions for Mg were determined with special care. In addition, to eliminate the presence of Pb-M multiple reflections, the pulse-height analyzer (PHA) was adjusted to differential mode operation with a proper, narrow energy-window setting. The background intensities under the peaks were calculated using the linear interpolation method. High analytical precision was achieved with counting times set sufficiently long to ensure a standard deviation due to Poisson counting statistics σ_c below 0.4% relative for all elements. Such requirements were achieved with typical counting times of about 50 s for Pb and Ti, and 80 s for Nb and Mg.

WDXS quantitative analysis was carried out using random sampling strategy: ten random areas were selected on the PMNT sample and in each area a group of ten random points positioned within a circle of $\approx$ 20-µm diameter was analyzed with two replicate measurements at each point. X-ray data from the quantitative measurements were also used to test the homogeneity of the sample on the macro-scale. The composition of the sample was determined from the elemental k-ratios, which were quantified using the $\Phi(\rho z)$ PROZA matrix-correction program [12], and for comparison using the conventional ZAF program as well [13a]. Mass absorption coefficient (MAC) values were taken after Heinrich [14]. It should be noted that the Pb-$M\alpha$ line (2.346 keV) is positioned close to the Nb-L_{III} absorption edge (2.371 keV). However, according to the Heinrich criteria, Pb-$M\alpha$ still lies outside the critical interval of -5 eV to 20 eV of an edge ($\Delta E=25$ eV) and consequently the corresponding MAC value may be used for reliable absorption calculations.

The micro-scale compositional homogeneity was tested with line-profile analyses performed at four randomly selected regions of the sample. X-ray data were acquired with WD spectrometers fixed at relevant
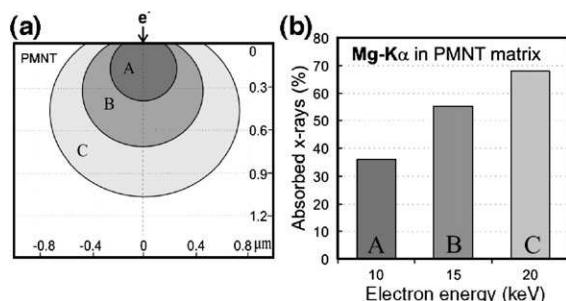

Fig. 1. Electron interaction volume (a) and fraction of absorbed Mg-$K\alpha$ radiation determined from the $\Phi(\rho z)$ distributions (b) for the PMNT matrix, as calculated from the Monte Carlo calculations for primary beam energies of 10 (A), 15 (B) and 20 (C) keV.
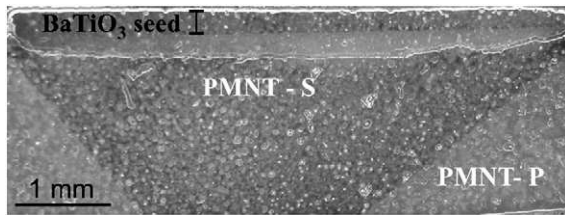
Fig. 2. Low-magnification view of the PMNT–BaTiO$_3$ cross-section showing the grown pyramid-like PMNT single-crystal part (S) and polycrystalline PMNT precursor (P).

X-ray peak positions to exclude any possible mechanical shift of the analyzing crystal during spectrometer repositioning from one element to another [15]. For every line profile, raw X-ray counts from 40 points with a step of 2 µm were measured at a 15-kV accelerating voltage, 60-nA beam current and 20-s counting time.

3. Results and discussion

3.1. Microstructure

A general view of the PMNT–BaTiO$_3$ sample cross-section is shown in Fig. 2. The PMNT single crystal (S) has grown from the porous polycrystalline matrix (P) in a pyramid-like shape. The crack present in the microstructure occurred artificially during the sample cross-section preparation. Due to the specific preparation technique the PMNT single crystal contains pores, which were left behind by the migrating boundary during crystal growth. The interface between the BaTiO$_3$ seed and PMNT was clear and sharp (Fig. 3). The dotted line marked in Fig. 3 represents the line-profile position for the analysis of the potential diffusion
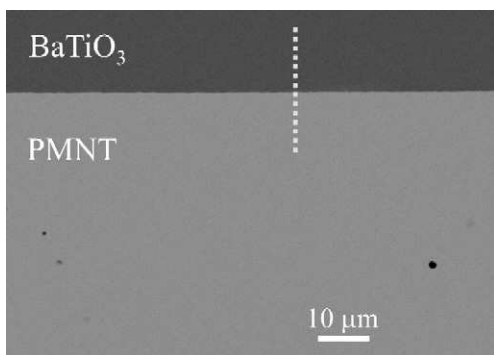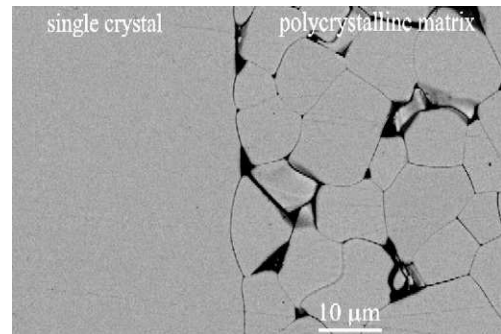

Fig. 4. SEM micrograph of the interface between the PMNT single crystal and the polycrystalline PMNT matrix.

between the seed and the crystal. The boundary between the polycrystalline matrix and the single crystal was observed after chemical etching of the sample using a solution of 2 vol.% HF and 4 vol.% HNO$_3$ in water, as shown in Fig. 4. Polycrystalline PMNT grains and grain boundaries became clearly visible, whereas the single-crystal surface remained unaffected. Further examination of the microstructure revealed the presence of some PbO-rich secondary phases (confirmed using EDXS) in the peripheral part of the crystal only (Fig. 5); these originate from the PbO excess added to the starting PMNT composition during the crystal preparation routine. The crystallographic orientation of the PMNT single crystal was checked with the EBSD patterns acquired from several positions on the crystal and from the BaTiO$_3$ seed, as well. All the patterns were equivalent and clearly demonstrate that the grown crystal retains the same crystallographic orientation as the seed. The corresponding orientation images with the main indexed patterns are shown in Fig. 6(a) and (b) respectively.

Fig. 3. SEM micrograph of the PMNT–BaTiO$_3$ interface recorded using backscattered electrons (BSE) and compositional contrast imaging.
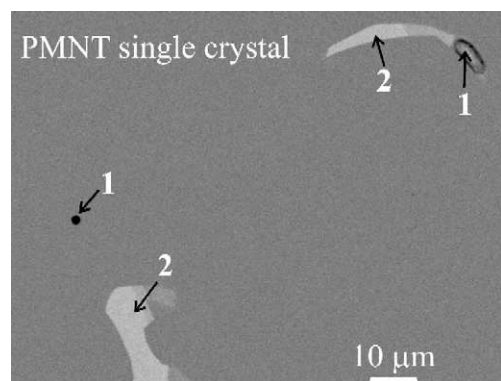

Fig. 5. SEM micrograph (BSE) of the PMNT single crystal part with marked pores (1) and PbO-rich secondary phases (2).
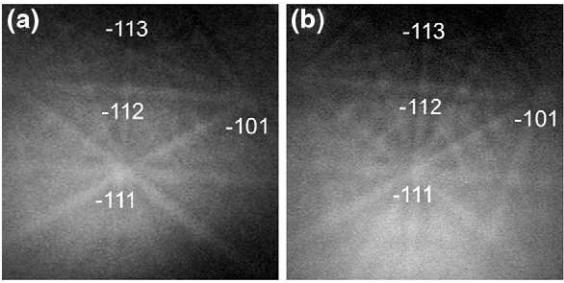
Fig. 6. EBSD patterns for orientation analysis acquired from the BaTiO$_3$ single-crystal seed (a) and from the grown PMNT single crystal (b). Equivalent patterns verify that the grown crystal retains the same orientation as the seed.

3.2. PMNT–BaTiO$_3$ interface

The diffusion between the BaTiO$_3$ (BT) seed and the PMNT crystal was investigated across the BT–PMNT boundary (see Fig. 3) using a semi-quantitative WDXS line-profile analysis consisting of 20 points and with a 1-μm step. Raw X-ray intensities plotted versus distance revealed that there is no noticeable diffusion between the seed and the grown crystal, as shown in Fig. 7. Apparent slight variations of the intensities observed close to the BT–PMNT boundary originate from mixed signals from both the BT and the PMNT due to the limited spatial resolution of the method, whereas signals measured for Mg, Pb and Nb on the BT side and for Ba on the PMNT side arise from the bremsstrahlung radiation (background).

3.3. Compositional analysis

A typical EDX spectrum acquired from the PMNT single crystal is shown in Fig. 8. The presence of related
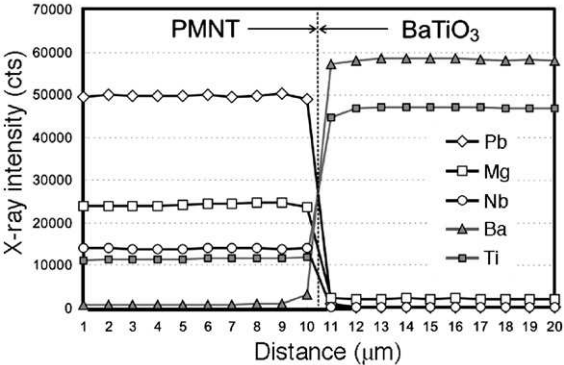

Fig. 7. Semi-quantitative WDXS line-profile analysis across the PMNT–BaTiO$_3$ boundary showing no interdiffusion between the PMNT crystal and the seed.
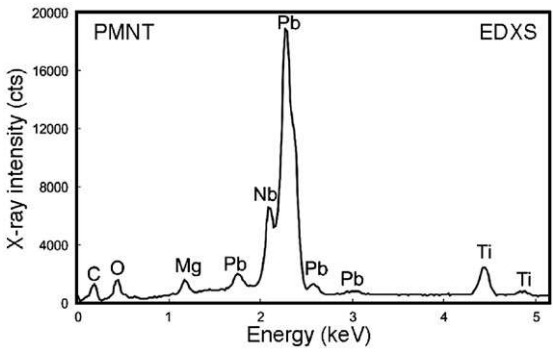

Fig. 8. The low-energy part (0–5 keV) of the EDX spectrum collected from the PMNT single crystal at 20 kV for 120-s acquisition time.

elements was clearly verified. Additionally, the spectrum revealed the strong peak overlap of the Pb-Mα and Nb-Lα spectral lines, which occurs due to the intrinsically low energy resolution of the method. This overlap represents the main problem for a correct quantitative analysis of Pb and Nb. Further drawbacks clear in the EDXS are the non-linear background under the Mg, Pb and Nb peaks, the presence of Nb-L$_{III}$ absorption edge under the overlapped Pb-Nb peaks, the large absorption of the Mg-Kα radiation in the PMNT matrix, the decreased efficiency of the energy-dispersive Si(Li) detector for-low energy spectral lines such as Mg-Kα, and the relatively low elemental peak-to-background ratios, which decrease the analytical sensitivity. All these issues can introduce substantial uncertainties when such energy-dispersive spectra are quantified. Nevertheless, for a further comparison with WDXS analyses, a semi-quantitative EDXS analysis was performed at five random points on the PMNT crystal. The spectra were quantified using the ZAF matrix-correction program and a "standardless" approach, with the reference spectra taken from a virtual standards package library. The results presented in Table 1 give the average elemental concentrations normalized to 100%, with the oxygen calculated from the stoichiometry. The reported experimental uncertainty (σ) was estimated

Table 1
EDXS quantitative analysis of the PMNT single crystal with given elemental concentrations (C) and experimental uncertainty (σ)

		Pb	Mg	Nb	Ti	O [a]
Average C	(wt.%)	64.00	1.30	13.55	5.70	15.45
σ	(wt.%)	±0.40	±0.06	±0.29	±0.14	–
Average C	(at.%)	19.40	3.36	9.16	7.48	60.61
Mg/Nb ratio		0.37				

[a] Calculated by stoichiometry.

Table 2
WDXS quantitative analysis of one typical group with ten random points on the PMNT single crystal with given average elemental concentrations (C) calculated from ten measured points

	Pb	Mg	Nb	Ti	O [a]	Total [b]
Average C (wt.%)	65.36	1.70	13.16	4.96	15.09	100.26
σ_{exp} (wt.%)	±0.23	±0.01	±0.04	±0.02	±0.02	±0.18
σ_{exp} (%)	0.35	0.75	0.34	0.34	0.11	0.18
σ^2_{wp} (wt.%)^2	0.01760	0.00010	0.00101	0.00013		
σ_{wp} (wt.%)	±0.133	±0.010	±0.032	±0.011		
σ^2_{bp} (wt.%)^2	0.03463	0.00006	0.00100	0.00016		
σ_{bp} (wt.%)	±0.186	±0.008	±0.032	±0.013		
MDL (wt.%)	0.051	0.003	0.023	0.005		
ΔC (wt.%)	0.143	0.004	0.041	0.011		
S^A (%)	0.25	0.36	0.48	0.27		
Average C (at.%)	20.00	4.43	8.98	6.57	60.02	
σ_{exp} (at.%)	±0.04	±0.02	±0.02	±0.01	±0.02	
Mg/Nb ratio	0.493±0.003					

[a] Calculated by stoichiometry.
[b] Non-normalized analytical total.

from the errors due to the counting statistics and to the variance between the analyzed points.

The total experimental uncertainty of the quantitative WDXS analysis for the elemental concentrations in wt.% was calculated from the corresponding components of variance according to the applied sampling method, as

$$\sigma_{exp} = \sqrt{\sigma^2_{wp} + \sigma^2_{bp} + \sigma^2_{bg}} \qquad (1)$$

where σ^2_{wp} is the variance within the points which originates from the experimental noise and is mainly associated with counting statistics, σ^2_{bp} is the variance between the points within a group and σ^2_{bg} is the variance between the groups. An examination of the quantitative data within individual groups of points revealed that all the cation concentrations are uniform, with negligible scattering observed between the points, as presented in Table 2 for one representative group. The non-normalized analytical totals close to 100% indicate the correctness of the applied analytical approach. An additional criterion for the consistency of the quantitative analysis was derived from the crystal chemistry expected for the complex PMNT solid solution. Namely, the B-sites in the PMNT perovskite structure are occupied by multiple ions Ti^{4+}, Mg^{2+} and Nb^{5+}, and the Ti^{4+} ions are substituted for the complex $(Mg_{1/3}Nb_{2/3})^{4+}$ [3]. Therefore, it is reasonable to assume that the ratio Mg/Nb = 0.5 should stay unchanged.

In contrast, an unequal occupation of the B-sites by means of a variation of the $Ti^{4+}/(Mg_{1/3}Nb_{2/3})^{4+}$ ratio can

take place during the crystal growth, which is a common phenomenon in crystals with multiple site occupancy grown from multi-component systems [3,4,7]. Consequently, the Mg/Nb atomic ratio was calculated and monitored as a significant parameter for the quantitative analyses. In the case of results given in Table 2, the measured Mg/Nb ratio of 0.493 is very close to the nominal one, with a discrepancy of only 1.4% relative.

The solid-solution formula was calculated from the elemental atomic % obtained from the measured wt.%, and by assuming that the oxygen is stoichiometric. Taking into account experimental uncertainty, the elemental concentrations fit perfectly to the ABO_3 perovskite formula, which is given by $Pb_{1.000±0.002}$ $(Mg_{0.221±0.001}Nb_{0.449±0.001})Ti_{0.328±0.001}O_3$.

X-ray data from the quantitative analysis performed on such uniform PMNT matrix were also taken to estimate the analytical precision of the method. Minimum detectability limit (MDL) values were calculated according to the Ziebold equation using the X-ray data measured on standards, whereas actual values for the achieved analytical sensitivity (ΔC) for a 95% confidence level were obtained using the X-ray data collected on the PMNT sample [16]. The analytical sensitivity (S^A) in percent was determined as $S^A = (\Delta C/C) \times 100$ (%), and conventionally should be ≤1% for a good analysis. For the results given in Table 2 the achieved values are even better and below 0.5% for all the elements. Both MDL and ΔC values were low and below the experimental uncertainty, indicating that a high analytical precision was achieved.

The analysis of variance and the statistical F-test for a 95% degree of confidence confirmed that the variances σ^2_{wp} and σ^2_{bp} are homogeneous within every group of ten points. From a statistical point of view, slight differences

Table 3
WDXS quantitative analysis of ten groups on the PMNT crystal with given grand average values for elemental concentrations (C) calculated from average values for every group

	Pb	Mg	Nb	Ti	O [a]
Grand average C (wt.%)	65.68	1.71	13.23	5.10	15.15
σ_{exp} (wt.%)	±0.33	±0.02	±0.17	±0.12	±0.04
σ_{exp} (%)	0.50	1.43	1.28	2.27	0.26
σ^2_{bg} (wt.%)^2	0.04811	0.00044	0.02394	0.01292	
σ_{bg} (wt.%)	±0.219	±0.021	±0.155	±0.114	
Grand average C (at.%)	19.90	4.42	8.94	6.69	60.05
σ_{exp} (at.%)	±0.08	±0.05	±0.10	±0.14	±0.03
Mg/Nb ratio	0.494±0.005				

[a] Calculated by stoichiometry.

Table 4
Calculated PMNT solid-solution formulas obtained from two analytical set-ups and two quantitative matrix correction methods

Analytical set-up	Matrix correction	PMNT solid-solution formula coefficients					Ratio Mg/ Nb
		Pb	Mg	Nb	Ti	O	
Analysis at 10 kV	ZAF	0.992	0.222	0.440	0.343	3	0.505
	PROZA	0.995	0.223	0.443	0.337	3	0.503
	σ	±0.004	±0.003	±0.004	±0.006		
Analysis at 15 kV	ZAF	0.995	0.216	0.443	0.340	3	0.486
	PROZA	0.994	0.221	0.447	0.334	3	0.494
	σ	±0.004	±0.003	±0.005	±0.007		

between the points and the average of the group were found to be insignificant.

For the comparison, the EDXS results (Table 1) gave underestimated values for Pb and Mg, overestimated values for Ti and Nb, a significantly lower Mg/Nb ratio of 0.37, a much higher experimental uncertainty and an erroneous formula $Pb_{0.97}(Mg_{0.17}Nb_{0.46})Ti_{0.37}O_3$.

The quantitative data for ten groups of points (Table 3) revealed increased scattering between the groups with measured deviations from the average composition of ±2.3% for Ti, ±1.4% for Mg, ±1.3% for Nb and only ±0.5% for Pb. The between-the-group variances σ_{bg}^2 (or σ_{bg}) for Mg, Nb and Ti were considerably higher, compared to the σ_{wp}^2 (σ_{wp}) and σ_{bp}^2 (σ_{bp}), indicating that a certain degree of heterogeneity across the crystal is present for the B-site cations. Additionally, the ANOVA evaluation of the σ_{bp}^2 and σ_{bg}^2 variances (calculated as "mean squares") confirmed that the differences between the group averages for Mg, Nb and Ti are statistically significant, whereas the differences for Pb were found to be insignificant.

The average PMNT solid-solution formula calculated from the overall (grand) average values of ten groups is given by $Pb_{0.994 \pm 0.004}$ $(Mg_{0.220 \pm 0.003}Nb_{0.447 \pm 0.005})$ $Ti_{0.334 \pm 0.007}O_3$. In addition, the comparison of the PMNT formulas obtained using quantitative results from two different analytical set-ups is presented in Table 4. For both set-ups the similar experimental uncertainty (σ) was obtained for formula coefficients. Consequently, the results in Table 4 show that, within the range of uncertainty, the PROZA matrix-correction program gave consistent results for the analyses performed at 15 kV and 10 kV. The ZAF program gave slightly higher values for Ti, and for an analysis at 15 kV underestimated values for Mg due to an insufficient absorption correction.

The occupancy of the B-site cations was determined for every group-average revealing an opposite trend in occupancy between the Ti^{4+} ions on one hand and the

Mg^{2+} and Nb^{5+} ions on the other, as shown in Fig. 9a. The graph of the relative B-site occupancy, calculated from the Ti/(Mg+Nb) ratio (Fig. 9b), confirms that a slightly unequal occupation of the B-sites is present over the entire grown PMNT crystal, with an average ratio of 0.5.

3.4. Compositional homogeneity

X-ray data from the micro-step line-profile analyses were tested for homogeneity using the expanded $\pm 3\sigma_c$ uncertainty interval, where $\sigma_c = \bar{N}^{1/2}$ is the counting error predicted from Poisson counting statistics and $\bar{N}$ is the average number of counts for a specific element in every profile. The simplified criterion states that the sample is assumed to be homogeneous if all the measured X-ray data points fall within the interval $\bar{N} \pm 3\sigma_c$. Therefore, the plots of raw X-ray intensities (N) versus distance with marked $\bar{N}$ and $\pm 3\sigma_c$ limits were used to reveal the compositional variations along the line profiles. Line profiles were recorded at four random positions, with
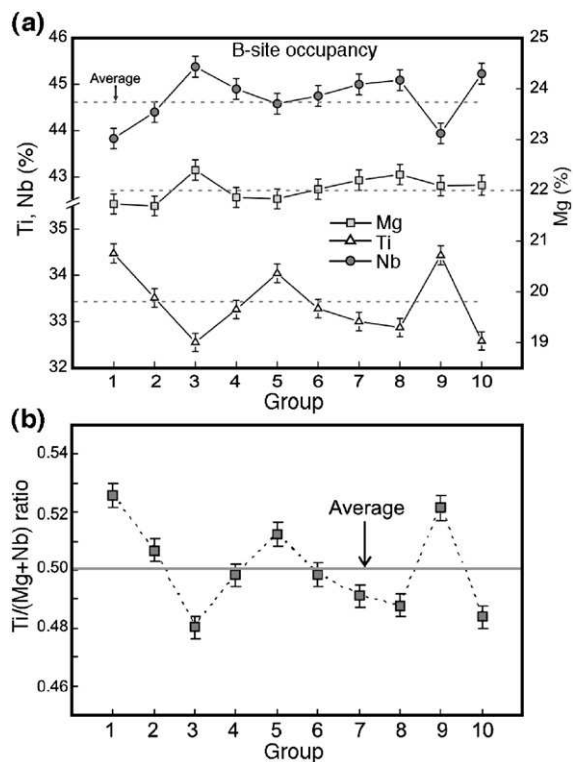

Fig. 9. (a) The occupancy of the B-sites by Ti^{4+}, Mg^{2+} and Nb^{5+} cations (in atomic %) calculated from quantitative results for ten groups. (b) The Ti/(Mg+Nb) atomic ratio reveals the variations of relative B-site occupancy between the groups across the PMNT crystal. Error bars represent $\pm 2\sigma$ where σ is calculated standard uncertainty.
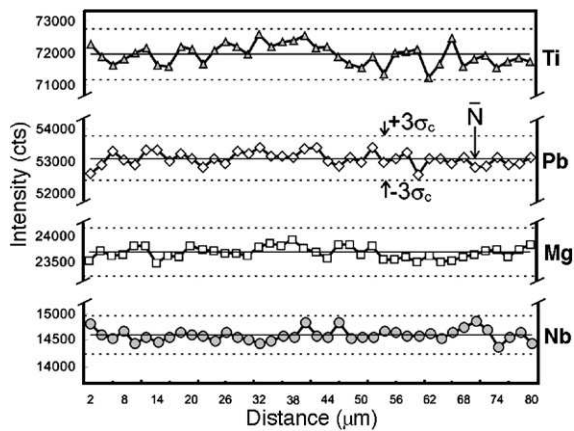
Fig. 10. Typical line-profile analysis for the compositional homogeneity study of the PMNT crystal on the μm-scale. All data points for all analyzed elements fall within the $\bar{N} \pm 3\sigma_c$ interval.

the typical concentration trends shown in Fig. 10, where all the data remain within the $\bar{N} \pm 3\sigma_c$ interval, thus confirming that the PMNT crystal appears to be compositionally homogeneous on the μm-scale. However, an "unusual" profile was also measured showing two opposite jumps, observed for Mg and Ti, as shown in Fig. 11. The explanation for such behavior is that in this case the line profile was accidentally positioned between two areas of the PMNT sample that abruptly differ in Mg and Ti concentrations, whereas the Pb and Nb concentrations remain uniform. Another very appropriate method to highlight the compositional variations is the use of distribution histogram plots. The X-ray data were sorted
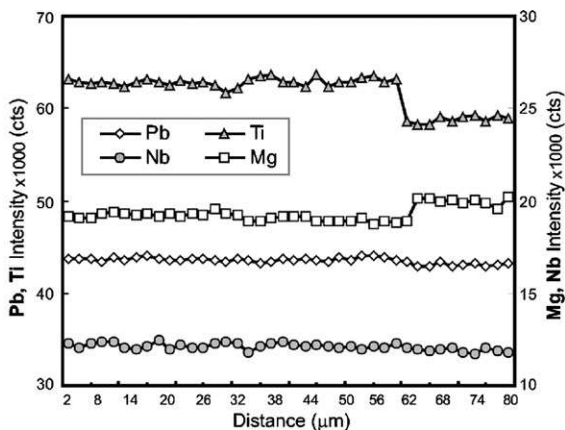

Fig. 11. An atypical line profile measured across two PMNT areas that differ in B-site cation concentrations showing an opposite change between Mg and Ti, while Pb and Nb remain uniform within both areas.
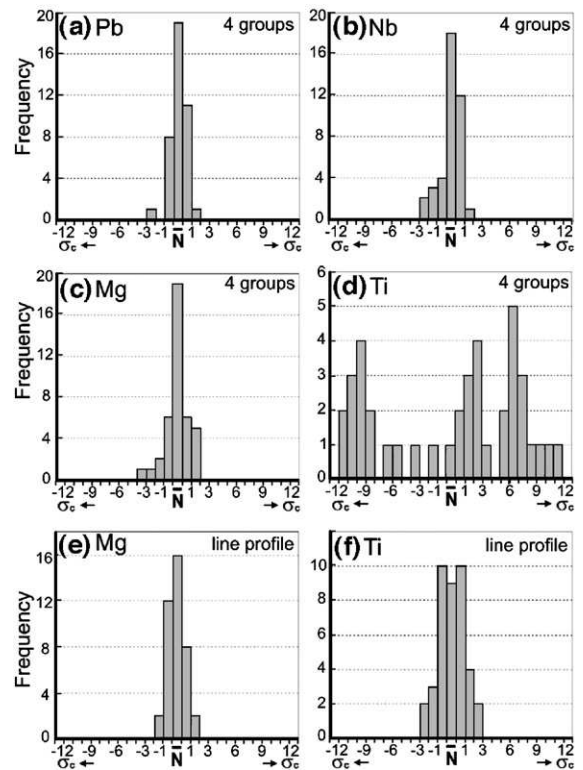

Fig. 12. Distribution histogram plots for Pb, Nb, Mg and Ti for the data collected from four random groups (a, b, c, d) compared with the data for Mg and Ti collected from the line-profile analysis (e, f). Histograms directly show that the largest scatter is present for Ti-data between the groups.

into the $\bar{N} \pm k\sigma_c$ ($k=1–13$) intervals and the frequency of the results versus the corresponding ranks was plotted. Such charts for data acquired from four different groups of points, where remarkable scatter was found, are shown in Fig. 12a, b, c, d. The histograms shown for Pb, Mg and Nb are narrow and suggest a more (Mg, Nb) or less (Pb) distorted Gaussian-like distribution, whereas the histogram for Ti reveals considerable scatter. It even seems like a mixture of three mutual distributions with the addition of some randomly scattered data points. For comparison, the Ti and Mg histograms (Fig. 12e, f) for a uniform part of the sample (data from line-profile analysis) are regular, with a Gaussian-like shape and with all the data within the $\bar{N} \pm 3\sigma_c$ interval.

A comprehensive study of the compositional homogeneity was undertaken using the data from both the line profiles and the quantitative analyses. Two sets of data, denoted as "micro" areas 1 and 2, were taken from the two line profiles. The other two sets of data, denoted as "macro" areas 1 and 2, were taken from the averages for ten groups and from an additional ten random points
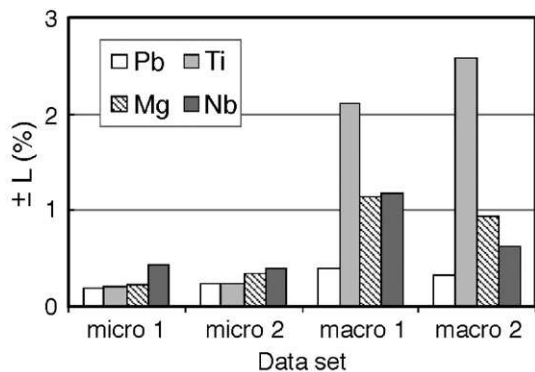
Fig. 13. The level of homogeneity (L) values calculated for two micro-areas and two macro-areas on the PMNT single crystal.

measured across the sample. For all data sets the level of homogeneity was calculated according to the formula [13b]

$$L = \pm \cdot \frac{t_{n-1}^{1-\alpha}}{\sqrt{n}} \cdot \frac{S_c}{\overline{N}} \cdot 100 \qquad (\%) \qquad (2)$$

where $t_{n-1}^{1-\alpha}$ is the Student t-value for a $1-\alpha$ confidence level and for $n-1$ degrees of freedom, n is the number of data points, $\overline{N}$ is the average number of counts and S_c is the standard deviation of n-measurements. It is usually accepted that the L-values for homogeneous materials should be below ±1%. The results for the PMNT sample L-values calculated for 99% degree of confidence ($\alpha = 0.01$) are presented in Fig. 13. The chart clearly shows that the L-values for the micro-areas are very low, and less than ±0.5% for all elements, thus confirming the compositional homogeneity of the PMNT crystal on the µm-scale. In contrast, for the macro-areas the L-values for the B-site cations increase and are especially high for Ti, whereas the values for Pb still remain very low. This indicates that a certain amount of heterogeneity for the Ti, Nb and Mg cations is present across the crystal, while Pb appears to be uniform. These results are in good agreement with the results of quantitative analyses, where similar compositional trends were predicted from the calculated components of variance.

4. Conclusions

A PMNT single crystal was grown from a polycrystalline PMNT matrix (70PMN–30PT) with PbO excess using the solid-state synthesis and templated grain-growth method with a $BaTiO_3$ single crystal as the seed. Microstructural analyses of the single crystal showed

the presence of pores and some PbO-based secondary phases. The boundary between the $BaTiO_3$ seed and the PMNT single crystal was sharp with no observable interdiffusion across the interface. The EBSD analysis revealed that the PMNT crystal had the same crystallographic orientation as the seed, thus confirming the heteroepitaxial crystal growth.

Qualitative EDXS analyses performed on the PMNT crystal verified the presence of related elements; however, quantitative results using the EDX spectra are unreliable and not accurate due to specific problems associated with the analysis of the PMNT sample.

The composition of the crystal was determined using an advanced EPMA–WDXS study optimized for the analysis of the PMNT matrix. The calculated average composition of the PMNT single crystal was $Pb_{0.994 \pm 0.004}$ $(Mg_{0.220 \pm 0.003}Nb_{0.447 \pm 0.005})Ti_{0.334 \pm 0.007}O_3$, and this fits well to the perovskite ABO_3 formula within the achieved experimental uncertainty.

The generalized solid-solution formula, described by $Pb(Mg_{1/3}Nb_{2/3})_{1-X}Ti_XO_3$, where $x = 0.33$, indicates that composition of the PMNT single crystal is very close to the MPB composition ($x \approx 0.35$), and that improved dielectric properties can be expected for such a PMNT material.

The high analytical sensitivity and the precision achieved with the EPMA allowed us to determine the composition of the PMNT crystal with a uncertainty better than 1% relative for all the analyzed elements. Within the localized areas the composition of the crystal was uniform, with a variation of less than 1% relative for all the elements, which falls within the experimental uncertainty of the method. On the macro-scale, compositional variations were found across the PMNT crystal, which were measured and statistically verified using the ANOVA, showing significant fluctuations for the B-site ions of ±2.3% for Ti, ±1.3% for Nb and ±1.4% for Mg. In contrast, the measured variation for Pb was negligible and within ±0.5% relative, indicating that Pb concentration was uniform over the entire crystal.

The measured variations for Ti^{4+}, Nb^{5+} and Mg^{2+} revealed that an unequal distribution of the B-site ions took place during crystal growth, with an opposite trend observed between the competing Ti and Mg–Nb ions. The calculated relative B-site occupancy indicates local composition fluctuations across the crystal, with an average atomic Ti/(Mg+Nb) ratio of 0.50 and a variation between 0.48 and 0.53 ($\approx \pm 5\%$ relative). This is a common phenomenon for such a complex PMNT material and similar solid solutions with a composition close to the MPB.

A detailed EPMA study using micro-step line-profile analyses confirmed that the PMNT single crystal was compositionally homogeneous on the μm-scale with a level of homogeneity below ±0.5% for all the elements. On the macro-scale the crystal possessed a certain degree of heterogeneity for Ti, Nb and Mg, with the largest scatter observed for Ti, whereas the Pb concentration was again found to be uniform, with the homogeneity level below ±0.5%. The results of the homogeneity study are highly consistent with the results obtained from the quantitative microanalysis.

A combined EPMA approach with an emphasis on optimized X-ray microanalysis has been successfully applied to investigate the microstructure, orientation and chemical composition of a PMNT single crystal. Since the slight compositional fluctuations could strongly affect the ferroelectric properties of PMNT materials, EPMA seems to be particularly useful for monitoring and measuring such possible fluctuations on the micro- and macro-scale with a high accuracy and precision. The results of the EPMA analyses of the PMNT crystal gave an important and complementary set of data, which can be further correlated with data obtained from thermodynamic, electrical, optical and structural characterization methods applied to advanced PMNT and related materials.

Acknowledgements

References

[1] Park S-E, Shrout TR. Ultrahigh strain and piezoelectric behaviour in relaxor based ferroelectric single crystals. J Appl Phys 1997;82(4):1804–11.

[2] Li T, Wu S, Khan A, Scotch AM, Chan HM, Harmer MP. Heteroepitaxial growth of bulk single-crystal $Pb(Mg_{1/3}Nb_{2/3})$ $O_3-32mol\%PbTiO_3$ from (111) $SrTiO_3$. J Mater Res 1999;14 (8):3189–91.

[3] Ye Z-G, Dong M. Morphotropic domain structures and phase transitions in relaxor-based piezo-/ferroelectric $(1-x)Pb(Mg_{1/3}$ $Nb_{2/3})O_3-xPbTiO_3$ single crystals. J Appl Phys 2000;87 (5):2312–9.

[4] Zawilski KT, Custodio MCC, DeMattei RC, Lee S-G, Monteiro RG, Odagawa H, Feigelson RS. Segregation during the vertical Bridgman growth of lead magnesium niobate-lead titanate single crystals. J Cryst Growth 2003;258:353–67.

[5] Guo Y, Luo H, He T, Xu H, Yin Z. Domain configuration and ferroelectric related properties of the $(110)_{cub}$ cuts of relaxor-based $Pb(Mg_{1/3}Nb_{2/3})O_3-PbTiO_3$ single crystals. Jpn J Appl Phys 2002;41:1451–4.

[6] Luo H, Xu G, Xu H, Wang P, Yin Z. Compositional homogeneity and electrical properties of lead magnesium niobate titanate single crystals grown by a modified Bridgman technique. Jpn J Appl Phys 2000;39:5581–5.

[7] Dong M, Ye Z-G. High-temperature solution growth and characterization of the piezo-/ferroelectric $(1-x)Pb(Mg_{1/3}Nb_{2/3}$ $)O_3-xPbTiO_3$ [PMNT] single crystals. J Cryst Growth 2000;209:81–90.

[8] Fan H, Zhao L, Tian C. Microstructure evolution of the templated grain growth in textured $Pb(Mg_{1/3}Nb_{2/3})_{0.67}Ti_{0.33}O_3$ by excess PbO addition. Ferroelectrics 2004;302:307–11.

[9] Lifshin E, Gauvin R. Minimizing errors in electron microprobe analysis. Microsc Microanal 2001;7:168–77.

[10] Lifshin E, Gauvin R. The role of Monte Carlo calculations in quantitative analysis. Microsc Microanal 1998;4:232–3.

[11] Hovington P, Drouin D, Gauvin R. CASINO: a new Monte Carlo code in C language for electron beam interactions – part I: description of the program. Scanning 1997;19:1–14.

[12] Bastin GF, Dijkstra JM, Heijligers HJM. PROZA 96: an improved matrix correction program for electron probe micro-analysis based on double Gaussian $\varphi(\rho z)$ approach. X-ray Spectrum 1998;27:3–10.

[13] Goldstein JI, Newbury DE, Echlin P, Joy DC, Romig AD, Lyman CE, Fiori C, Lifshin E. Scanning Electron Microscopy and X-Ray Microanalysis. Plenum Press, New York: 1992, (a) p. 417–434; (b) p. 497.

[14] Heinrich KFJ. Mass absorption coefficients for electron probe microanalysis. Proc 11th Int Conf of X-ray Optics and Microanalysis. London, Ontario, Canada, August 4–8; 1987.

[15] Marinenko R, Leigh S. Heterogeneity evaluation of research materials for microanalysis standards certification. Microsc Microanal 2004;10:491–506.

[16] Ziebold TO. Precision and sensitivity in electron probe microanalysis. Anal Chem 1967;39:858–61.